NANO LETTERS

2004
Vol. 4, No. 12
2343−2347

DNA-Templated Self-Assembly of Metallic Nanocomponent Arrays on a Surface

John D. Le,[†] Yariv Pinto,[†,‡] Nadrian C. Seeman,[§] Karin Musier-Forsyth,[‡] T. Andrew Taton,[‡] and Richard A. Kiehl*[,†]

Department of Electrical and Computer Engineering and Department of Chemistry, University of Minnesota, Minneapolis, Minnesota 55455, and Department of Chemistry, New York University, New York, New York 10003

Received August 23, 2004; Revised Manuscript Received October 2, 2004

ABSTRACT

A method for laying out arrays of components in programmable 2D arrangements with nanometer-scale precision is needed for the manufacture of high density nanoelectronic circuitry. We report programmed self-assembly of gold prototype nanoelectronic components into closely packed rows with precisely defined inter-row spacings by in situ hybridization of DNA-functionalized components to a preassembled 2D DNA scaffolding on a surface. This approach is broadly applicable to the manufacture of nanoscale integrated circuits for logic, memory, sensing, and other applications.

While some components in a microprocessor are laid out in a nearly random arrangement dictated by logic design, many arithmetic building blocks and circuit subsystems are laid out in regular two-dimensional (2D) arrays.[1] Two important examples of subsystem arrays are the dynamic random-access memory (DRAM), which is the main read/write memory in computers and the most highly produced electronic device, and the programmable logic array (PLA), which allows arbitrary logic functions to be implemented in a regular array of components. Regular 2D arrays will play an expanding role in future generations of microprocessors, where memory will occupy an increasing fraction of the chip area, and in new paradigms for nanoelectronic circuitry, where the limited drive capability of small devices and limits on power dissipation at high integration levels will mandate architectures based on more locally connected arrays.[2,3] Thus, a process for the manufacture of 2D nanocomponent arrays with programmable component spacing and precise registry would enable the development of a wide variety of nanoelectronic integrated circuits.

Self-assembly by DNA scaffolding is a bottom-up approach for arranging nanometer-scale components with a theoretical precision of 0.34 nm, the separation between base pairs in a B-form, double-stranded DNA helix. Moreover, DNA offers programmability in the arrangement of nanocomponents through base sequence design. Gold nanoparticles attached to single-stranded DNA molecules have been assembled into dimers and trimers by sequence-specific DNA hybridization,[4] and straight chains of 5 to 10 nanoparticles have been formed from streptavidin-labeled Au particles and biotin-containing DNA templates.[5] Two-dimensional DNA crystals, first described in 1998,[6] provide attractive templates for organizing nanocomponents into regular 2D geometries. Such 2D DNA crystals have been used to organize other DNA molecules[7] and protein molecules[6,8] into predetermined patterns in which the molecules are bound to periodic binding sites on the array. In earlier work by members of our group, metallic nanocomponents were incorporated into a 2D DNA crystal during crystal growth through their prior covalent attachment to one of the DNA strands making up the crystal.[9] Here, we demonstrate the self-assembly of metallic nanocomponents into high density 2D arrays by a process in which DNA−Au nanocomponents are hybridized to a pre-assembed 2D DNA scaffolding in situ on a solid surface. In this way, many thousands of DNA sequence-encoded nanoelectronic components are organized into regular arrays with defined particle locations and interparticle spacing. This approach provides an adaptable method for in situ self-assembly of 2D nanoelectronic component arrays and their integration with other structures, devices, and circuits.

The 2D DNA scaffolding in this study is constructed from a set of 21 synthetic oligonucleotides that are designed to assemble into four different double-crossover (DX) tiles: A, B, C, and D (Figure 1). The scaffolding design closely

* Corresponding author. E-mail: kiehl@ece.umn.edu.
[†] Department of Electrical and Computer Engineering, University of Minnesota.
[‡] Department of Chemistry, University of Minnesota.
[§] Department of Chemistry, New York University.

10.1021/nl048635+ CCC: $27.50
Published on Web 10/29/2004

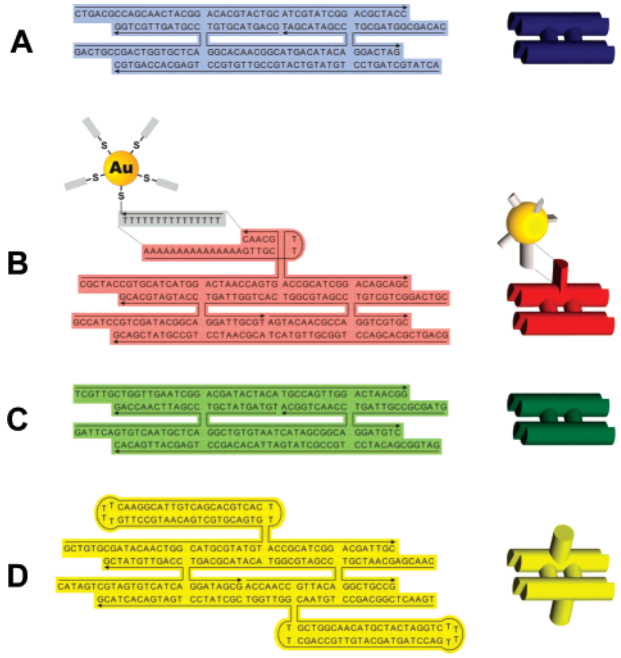

Figure 1. Base sequence schematics and geometric models for the DX subunits and DNA−Au nanocomponent. The intermolecular interactions between these structural units, or "tiles", are programmed by the design of "sticky ends" that associate by Watson−Crick pairing. The spherical Au nanoparticle bears multiple, identical DNA strands (typically 5−10 strands per molecule) that are complementary to the hybridization site on tile B. Arrowheads indicate the 3′ ends of the strands. The sequence is shown on one strand only, and one strand is elongated in the model for clarity. A unique color is chosen for each DX tile type and corresponds to that used in the illustrations of the assembled scaffolding (Figure 2).

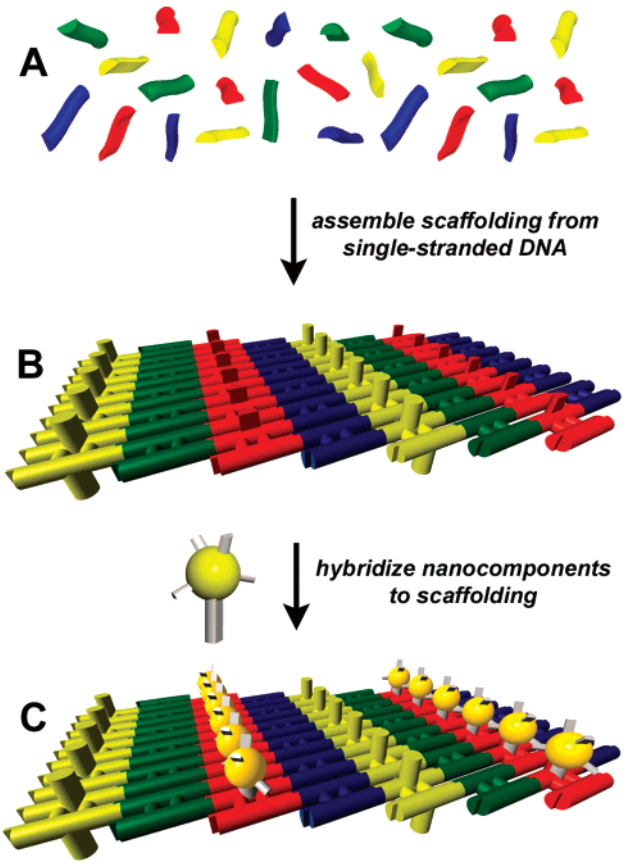

Figure 2. Assembly steps for the 2D nanocomponent arrays. (A) The DNA scaffolding is first assembled in solution from the set of 21 strands. (B) A suspension of the DNA scaffolding is deposited on mica, allowing the scaffolding to attach to the surface. The scaffolding is composed entirely of double-stranded DNA, except for the open, single-stranded hybridization sites on the B tiles (red). DNA hairpin topological markers extend from the D tiles (yellow). (C) The scaffolding is combined with DNA-encoded nanocomponents, which attach to the open hybridization sites. While this diagram shows one nanocomponent occupying each site, single nanoparticles can also attach to multiple sites via hybridization of multiple, nanoparticle-bound strands.

resembles that described by Liu et al.,[7] and the dimensions of the tiles are about 2 nm × 4 nm × 16 nm. Tile B includes an extended single-stranded DNA feature that is designed to hybridize to oligonucleotides bound to nanocomponents (Figure 1B). Tile D includes extended structures composed of DNA hairpins above and below the crystal plane, which are used as topographical markers on the crystal (Figure 1D).

The nanoelectronic component in this study is composed of a 6-nm Au nanoparticle functionalized with multiple strands of 3′-thiolated $(dT)_{15}$ (Figure 1B). These DNA−Au conjugates were prepared from 3′-thiol-modified-$(dT)_{15}$ and 5-nm-diameter Au nanoparticles (BBI International) according to published procedures.[10,11] The 15-thymine base sequence is complementary to the 15-adenine base sequence of the hybridization site on the DX tile B. Both the multiple functionalization of the Au nanoparticle and the use of identical bases, rather than a mixed sequence of bases, are potentially advantageous to nanocomponent attachment in this case since they provide a greater degree of freedom in the hybridization to the scaffolding. Multiple functionalization allows the attachment of each nanoparticle through more than one strand. The use of identical bases allows the complementary strands to slide along one another and to bind with a variable number of bases, thereby accommodating the crowding of the strands near the particle and the scaffolding which might otherwise interfere with the hybridization.

The self-assembly of Au nanocomponent arrays was performed in three steps. First, the DNA scaffolding was grown by slowly cooling a buffered solution containing a stoichiometric mixture of the 21 strands from 90 °C to room temperature (Figure 2A). During cooling, the single-stranded DNA assembles into the four DX tiles, and these tiles further assemble by sticky-ended cohesion to tile the plane, thereby forming a suspension of 2D crystals. Second, a 4-μL drop of the DNA scaffolding suspension was deposited on freshly cleaved mica and allowed to adsorb to the surface for approximately 1 min. The buffer salts were rinsed away with 100 μL of doubly distilled water, and the sample was blown dry with nitrogen (Figure 2B). Finally, a 4-μL volume of 0.2 μM DNA−Au conjugate in TAEMg buffer (20 mM tris, 20 mM acetic acid, 2 mM EDTA, 12.5 mM magnesium acetate) was deposited on the mica substrate and allowed to hybridize for 5 min. The surface was then rinsed in 100 μL

of water and blown dry with nitrogen (Figure 2C). The scaffolding is designed to form rows of hybridization sites on the crystal with a 4-nm spacing between sites and a 64-nm separation between rows; the sequences also form DNA hairpin rows that alternate with the hybridization rows and have identical spacing and separation (Figures 2B, 2C).

Topographical atomic force microscopy (AFM) images of the DNA scaffolding on mica prior to the hybridization step show ridges of alternating height with a separation of ~63 nm between ridges of similar height (Figures 3A, 3C). The measured heights of the two sets of ridges are ~1.7 and ~1.0 nm (Figure 3G). We attribute these features to alternating rows of the relatively high DNA hairpin markers on tile D (Figure 1D) and the smaller DNA hybridization sites on tile B (Figure 1B). AFM images of samples taken after the nanocomponent hybridization step reveal an assembly of particles along lines on the scaffolding (Figures 3B, 3D). The particles form closely packed rows separated by ~63 nm, and ridges are observed midway between the rows. The measured particle height is ~7 nm (Figure 3H), in good agreement with the expected height of a 6-nm hard Au particle with a soft single-stranded DNA shell on a soft DNA scaffold layer. (The width of the dots in an AFM image is related to the probe-tip curvature, and hence does not reflect the actual particle size.) The height of the ridge between the particles is ~1.5 nm (Figure 3H), which is approximately the height of DNA marker measured prior to the hybridization step (Figure 3G).

To prove that the nanocomponents are attached to the scaffolding through Watson−Crick hybridization, rather than through a nonspecific interaction, we carried out a control experiment using the same DNA−Au nanocomponent and a DNA scaffolding that was identical to the original design (Figure 1), except that the $(dA)_{15}$ hybridization site was replaced with a random noncomplementary base sequence. In this design, the hybridization site on the scaffolding is not complementary to the $(dT)_{15}$−Au oligomer, and attachment to the array should not occur if hybridization is the predominant binding process. AFM images of the DNA scaffolding on mica before the hybridization step for the control structure (Figure 3E) are similar to those for the original structure (Figures 3A, 3C). In contrast, virtually no nanocomponents are found on the scaffolding after the hybridization step for the control (Figure 3F; compare with Figures 3B and 3D). In fact, we find that noncomplementary DNA-modified nanoparticles are repelled by the DNA array and settle onto the positively charged mica surface (Figure 3F),[12] presumably as a result of mutual anionic charge repulsion between DNA strands. This control experiment supports our conclusion that Watson−Crick base pairing drives the assembly of nanocomponents on the scaffolding.

While topographical AFM provides a detailed 3D visualization of the assembled structure (Figure 4A), the AFM images lack information regarding material composition. To prove that the assembled rows of dots are DNA−Au nanocomponents, rather than DNA structures alone, we examined the samples by transmission electron microscopy (TEM), which provides an image with electron-density dependent contrast that allows metallic structure to be identified. The TEM image confirms that rows of closely

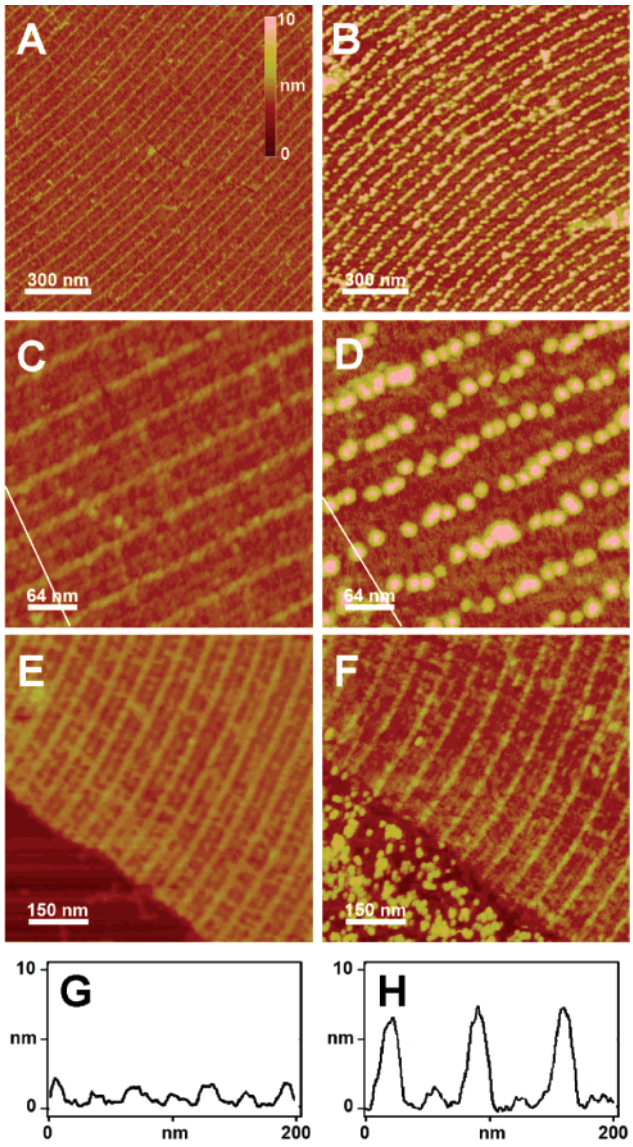

Figure 3. DNA scaffolding before and after the hybridization step. (A and C) Topographical AFM images of the DNA scaffolding before the nanocomponent hybridization step. Brighter (taller) diagonal ridges correspond to rows of the topographical marker hairpins attached to tile D, and fainter (shorter) ridges to rows of single-stranded hybridization sites on tile B. The measured spacing between tile D ridges is 64.3 ± 2.7 nm. (B and D) AFM images of the DNA scaffolding after nanocomponent assembly. Nanocomponents attach to only the shorter ridges in images (A) and (C). (E and F) Control experiment to confirm the nanocomponent hybridization specificity. AFM image before (E) and after (F) the (dT)-15-Au hybridization step for a control scaffolding that is identical in design to the original scaffolding (Figures 1 and 2) except that the hybridization-site sequence is not complementary to the nanocomponent sequence. For both (E) and (F), sample preparation and nanocomponent reaction conditions were identical to those used for the original design. (G) Height profile along the line shown in image (C). The heights of the two sets of ridges are 1.7 ± 0.2 nm and 1.0 ± 0.1 nm. (H) Height profile along the line shown in image (D). The height of the nanocomponents and the remaining visible ridge measure 7.1 ± 0.5 nm and 1.5 ± 0.2 nm, respectively. All AFM images were obtained on a Digital Instruments Mulitmode III in 2-propanol using an oxide-sharpened silicon-nitride cantilever.

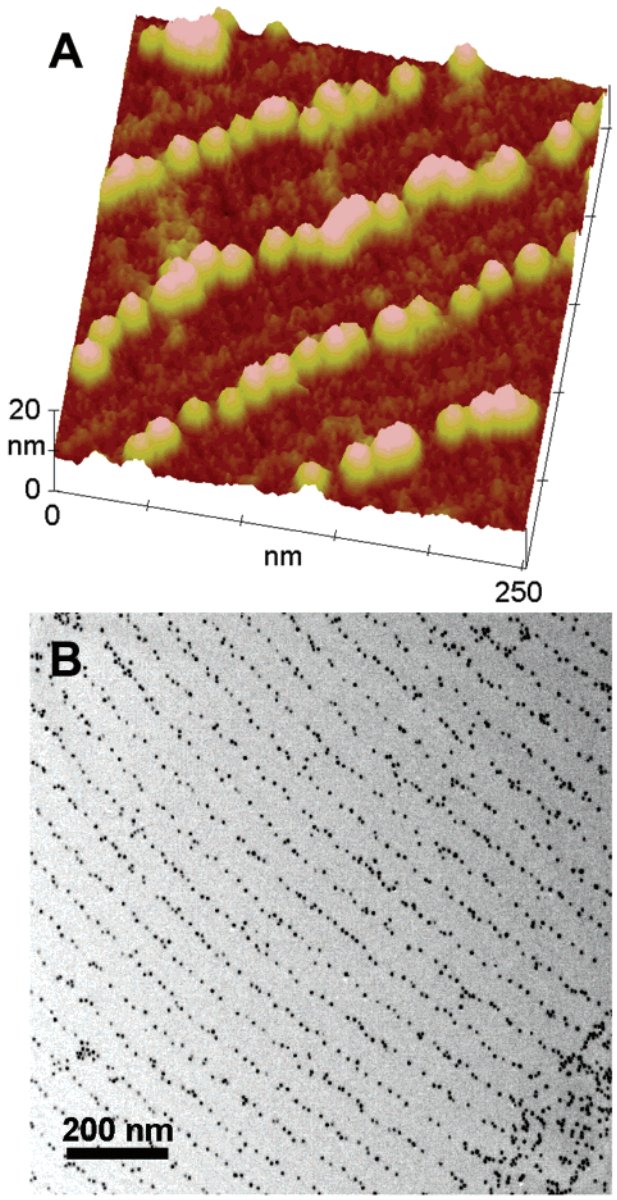

Figure 4. Visualization of the DNA−Au nanocomponent arrays. (A) Topographical AFM image of an assembled array providing a 3D visualization of the assembled DNA−Au nanocomponents, DNA marker rows, and DNA scaffolding. (B) TEM image of the nanocomponent array. The high-contrast particles in the image measure 6.2 ± 0.8 nm in diameter. The center-to-center particle spacing is typically in the range of 15 to 25 nm and is 12.0 ± 3.0 nm in close-packed regions. The average spacing between rows is 62.9 ± 0.8 nm. The TEM sample was prepared by transferring the nanoparticle arrays prepared on a mica substrate to a copper-mesh TEM grid. The transfer was facilitated by a thin carbon support layer that was evaporated on the mica substrate and lifted off by immersion in buffer solution. The TEM sample was imaged on a Philips CM30 operated at 300 kV.

spaced metallic (high-contrast) particles with a ∼6-nm diameter have been assembled with an inter-row spacing of ∼63 nm (Figure 4B). The average spacing between particles along rows in typical regions is ∼20 nm, whereas the spacing in closely packed regions is ∼12 nm. This latter spacing is about 3 times the hybridization site spacing and may represent the effective size of the nanocomponent on the scaffolding surface commensurate with its 6-nm Au core and single-stranded DNA shell. Because the particles are larger than the hybridization site spacing on the crystal, each multiply functionalized nanoparticle may be connected to multiple hybridization sites on the array.

This method for the programmed self-assembly of metallic nanocomponents into regular arrays is suitable for fundamental studies of nanoscale manufacturing and of the electronic properties (electron tunneling, Coulomb blockade, quantum-size effects) of inorganic/organic nanoscale systems. In contrast to our previously reported method for the assembly of metallic nanocomponents by their incorporation into DNA scaffolding during its growth,[9] the present method permits the independent optimization of the DNA crystal growth conditions and the component synthesis conditions, which allows the technique to be extended to a wide range of applications. While we have chosen a nanocomponent that is larger than the spacing between hybridization sites along the rows, applications requiring the positioning of a single nanocomponent at each hybridization site could be accommodated by appropriate design of the periodicity of the DNA scaffolding and the size of the components. Greater precision in the control of the final structure also could be obtained through the use of nanocomponents functionalized with a single DNA molecule.

A near-term application for the 2D array fabricated here is a high capacity memory in which the electronic or magnetic state of each metallic nanocomponent is accessed by scanning probe technology.[13] Other applications include nanoscale sensor arrays,[14] field-programmable gate-arrays,[15] and cellular nonlinear networks.[16] Because the general approach described here could be applied to different kinds of DNA-encoded nanocomponents (with other material compositions and electronic properties), and to DNA templates with other geometrical arrangements,[17,18] this method could be used to fabricate a variety of more complex, multicomponent devices and circuitry. This approach for assembling *nanometer-scale* components into *micrometer-scale* arrays on a surface suggests a promising strategy for integrating nanoelectronics with the microelectronics world.

Acknowledgment. This work was supported by NSF Nanoscale Interdisciplinary Research Team (NIRT) Grant NSF/DMI-0210844.

Supporting Information Available: DX tile design, assembly of DNA scaffolding, and detailed DNA sequences. This material is available free of charge via the Internet at http://pubs.acs.org.

References

(1) Rabaey, J. M.; Chandrakasan, A.; Nikolic, B. *Digital Integrated Circuits*; Prentice Hall: New York, 2003.
(2) Semiconductor Industry Association, "International Technology Roadmap for Semiconductors," 2003 (http://public.itrs.net/).
(3) Kiehl, R. A. *J. Nanopart. Res.* **2000**, *2*, 331−332.
(4) Alivisatos, A. P.; Johnsson, K. P.; Peng, X.; Wilson, T. E.; Loweth, C. J.; Bruchez, M. P.; Schultz, P. G. *Nature* **1996**, 609−611.
(5) Li, H.; Park, S. H.; Reif, J. H.; LaBean, T. H.; Yan, H. *J. Am. Chem. Soc.* **2004**, *126*, 418−419.

(6) Winfree, E.; Liu, F.; Wenzler, L. A.; Seeman, N. C. *Nature* **1998**, *394*, 539−544.
(7) Liu, F.; Sha, R.; Seeman, N. C. *J. Am. Chem. Soc.* **1999**, *121*, 917−922.
(8) Yan, H.; Park, S. H.; Finkelstein, G.; Reif, J. H.; LaBeam, T. H. *Science* **2003**, *301*, 1882−1884.
(9) Xiao, S. J.; Liu, F. R.; Rosen, A. E.; Hainfeld, J. F.; Seeman, N. C.; Musier-Forsyth, K.; Kiehl, R. A. *J. Nanopart. Res.* **2002**, *4*, 313−317.
(10) Taton, T. A. *Curr. Protocols Nucleic Acids Chem.* **2001**, *12.2*, 1−12.
(11) Storhoff, J. J.; Elghanian, R.; Mucic, R. C.; Mirkin, C. A.; Letsinger, R. L. *J. Am. Chem. Soc.* **1998**, *120*, 1959−1964.
(12) Kasas, S.; Thomson, N. H.; Smith, B.; Hansma, H. G.; Hansma, P. K. *Langmuir* **1996**, *12*, 5905−5908.
(13) Born, A.; Wiesendanger, R. *Appl. Phys. A* **1999**, *68*, 131−135.
(14) Hagleitner, C.; Hierlemann, A.; Lange, D.; Kummer, A.; Kerness, N.; Brand, O.; Baltes, H. *Nature* **2001**, *414*, 293−296.
(15) Heath, J. R.; Kuekes, P. J.; Snider, G. S.; Williams, R. S. *Science* **1998**, *280*, 1716−1721.
(16) Yang, T.; Kiehl, R. A.; Chua, L. O. *Int. J. Bifurc. Chaos* **2001**, *11*, 2895−2911.
(17) Sa-Ardyen, P.; Vologodskii, A. V.; Seeman, N. C. *Biophys. J.* **2004**, *84*, 3829−3837.
(18) Liu, D.; Wang, M.; Deng, Z.; Walulu, R.; Mao, C. *J. Am. Chem. Soc.* **2004**, *126*, 2324−2335.

NL048635+